2016

Single Nanoparticle Plasmonic Spectroscopy for Study of the Efflux Function of Multidrug ABC Membrance Transporters of Single Live Cells

Lauren M. Browning
Old Dominion University

Kerry J. Lee
Old Dominion University

Pavan K. Cherukuri
Old Dominion University

Prakash D. Nallathamby
Old Dominion University

Seth Warren
Old Dominion University

See next page for additional authors

Original Publication Citation

Browning, L. M., Lee, K. J., Cherukuri, P. K., Nallathamby, P. D., Warren, S., Jault, J. M., & Xu, X. H. N. (2016). Single nanoparticle plasmonic spectroscopy for study of the efflux function of multidrug ABC membrane transporters of single live cells. *RSC Advances, 6*(43), 36794-36802. doi:10.1039/c6ra05895g

RSC Advances

PAPER

View Article Online
View Journal | View Issue

Cite this: *RSC Adv.*, 2016, **6**, 36794

Single nanoparticle plasmonic spectroscopy for study of the efflux function of multidrug ABC membrane transporters of single live cells†

Lauren M. Browning,[a] Kerry J. Lee,[a] Pavan K. Cherukuri,[a] Prakash D. Nallathamby,[a] Seth Warren,[a] Jean-Michel Jault[b] and Xiao-Hong Nancy Xu*[a]

ATP-binding cassette (ABC) membrane transporters exist in all living organisms and play key roles in a wide range of cellular and physiological functions. The ABC transporters can selectively extrude a wide variety of structurally and functionally unrelated substrates, leading to multidrug resistance. Despite extensive study, their efflux molecular mechanisms remain elusive. In this study, we synthesized and characterized purified silver nanoparticles (Ag NPs) (97 ± 13 nm in diameter), and used them as photostable optical imaging probes to study efflux kinetics of ABC membrane transporters (BmrA) of single live cells (*B. subtilis*). The NPs with concentrations up to 3.7 pM were stable (non-aggregated) in a PBS buffer and biocompatible with the cells. We found a high dependence of accumulation of the intracellular NPs in single live cells (WT, Ct-BmrA-EGFP, ΔBmrA) upon the cellular expression level of BmrA and NP concentration (0.93, 1.85 and 3.7 pM), showing the highest accumulation of intracellular NPs in ΔBmrA (deletion of BmrA) and the lowest ones in Ct-BmrA-EGFP (over-expression of BmrA). Interestingly, the accumulation of intracellular NPs in ΔBmrA increases nearly proportionally with the NP concentration, while those in WT and Ct-BmrA-EGFP do not. This result suggests that the NPs enter the cells *via* passive diffusion driven by concentration gradients across the cellular membrane and they are extruded out of cells by BmrA transporters, similar to conventional pump substrates (antibiotics). This study shows that such large substrates (84–100 nm NPs) can enter into the live cells and be extruded out of the cells by BmrA, and the NPs can serve as nm-sized optical imaging probes to study the size-dependent efflux kinetics of membrane transporters in single live cells in real time.

Received 5th March 2016
Accepted 17th March 2016

DOI: 10.1039/c6ra05895g

www.rsc.org/advances

Introduction

ABC membrane transporters (efflux pumps) are involved in the transport of a wide variety of structurally and functionally unrelated substrates (*e.g.*, sugars, lipids, aminoacids, proteins, and xenobiotics), including extrusion of antibiotics or chemotherapeutic agents out of cells (*e.g.*, bacteria or tumor cells), which leads to ineffective treatment of infection and cancer.[1,2] The ABC transporters share a common organization and suggest possible similar transport mechanisms.[3–6] Majority of ABC transporters include four core domains: two transmembrane domains (TMD) with variable sequence and topology and two nucleotide-binding domains (NBD) with conserved sequences.[3–6] The TMDs define the substrate binding-sites and form the transport passageway for substrates to cross the membranes, while the NBDs bind and hydrolyze ATP to power the transporters.[3,4,7,8]

Currently, radioactively labeled substrates (^{14}C and ^{3}H) and the fluorescence dyes (*e.g.*, rhodamine 123, Fluo-3, Hoechst dyes) have served as popular probes for study of efflux kinetics of multidrug transporters in both bacterial and mammal cells.[9–15] These conventional methods enable one to study ensemble accumulation kinetics of bulk cells. We have also demonstrated that thin-layer total-internal reflection fluorescence microscopy and spectroscopy can be used to measure efflux kinetics of single membrane transporters of single live cells in real-time.[13] However, fluorophores cannot be used to determine transformation of pore sizes of membrane transporters in response to various sizes of substrates in single live cells. Therefore, they are unable to study size-dependent efflux kinetics of multidrug (multi-substrate) membrane transporters. These limitations demand the development of new probes and methods to study the size-dependent efflux functions of individual membrane transporters in single live cells in real time, in order to better understand underlying molecular mechanisms of multidrug membrane transporters. Notably, individual

[a]*Department of Chemistry and Biochemistry, Old Dominion University, Norfolk, VA 23529, USA. E-mail: xhxu@odu.edu; Web: http://www.odu.edu/sci/xu/xu.htm; Fax: +1 757 683 5698; Tel: +1 757 683 5698*

[b]*UMR5086 CNRS/UCBLyon I, MMSB-IBCP, 7 Passage du Vercors, 69367 Lyon cedex 07, France*

† Electronic supplementary information (ESI) available. See DOI: 10.1039/c6ra05895g

membrane transporters and single live cells act distinctively, underscoring the importance to study the transport kinetics of single membrane transporters in single live cells in real time.

Structures and sizes of a few membrane transporters have been characterized at atomic resolution using X-ray crystallography or cryo-TEM.[3,5,16,17] However, current methods cannot measure real-time transport dynamics of substrates and self-assembly of pump proteins in live cells. Therefore, despite extensive studies, the mechanisms and efflux functions of membrane transporters remain elusive.

Noble metal nanoparticles, such as silver nanoparticles (Ag NPs), show size-dependent plasmonic optical properties.[18–20] The Ag NPs show orders of magnitude higher scattering intensity than the same sized of Au NPs.[18–23] Furthermore, single Ag NPs exhibit much higher size-dependent localized surface plasmon resonance (LSPR) spectra than Au NPs.[18–23] Therefore, Ag NPs are much more sensitive optical imaging probes for the study of size-dependent efflux kinetics of membrane transporters in single live cells than the Au NPs. We have used the size-dependent LSPR spectra (colors) of single Ag NPs to image the sizes of NPs in solution, single live cells and embryos at nm resolution in real time.[20,23–27]

Unlike fluorescent probes and semiconductor quantum dots (QDs), these noble metal NPs show superior photostability and resist photodecomposition and blinking and they can serve as optical probes for tracking the transformation of pore sizes of membrane transporters and the size-dependent transport kinetics of efflux pumps for a desired period of time.[24–26]

We have previously used size-dependent plasmonic optical properties of the noble metal NPs to study size-dependent transport dynamics of single membrane transporters (MexAB-OprM) in single live cells (*P. aeruginosa*, Gram negative bacterium), and to determine the transformation of pore sizes of their cellular membranes induced by antibiotics (*e.g.*, aztreonam, chloramphenicol) at sub-100 nm spatial resolution and millisecond temporal resolution.[24–26,28]

We have also used smaller Ag NPs (11.8 ± 2.6 nm) to study the efflux kinetics of BmrA (ABC) membrane transporters in *B. subtilis* (a Gram-positive bacterium).[29] Notably, *B. subtilis* has served as a popular model organism for study of efflux function of multidrug ABC membrane transporters, and 78 ABC transporters have been identified in *B. subtilis*.[30–32] In our previous study,[14,29] we have constructed two new strains of *B. subtilis*, BmrA fused with EGFP *via* its C- or N-terminus (Ct-BmrA-EGFP or Nt-BmrA-EGFP) and characterized their efflux function using smaller Ag NPs (11.8 ± 2.6 nm) and fluorophore (Hoechst dyes). We found that both mutants retain the efflux function of BmrA.[14,29]

In this study, we synthesized and characterized larger Ag NPs (97 ± 13 nm), and used their size-dependent LSPR spectra to determine the sizes of single NPs at nm resolution in real time as they are in and out of single live cells, and to study size-dependent efflux kinetics of BmrA of single live bacterial cells (*B. subtilis*). The study of size-dependent efflux function of membrane transporter is essential to address multidrug resistance. The LSPR spectra of single Ag NPs highly depend upon its size, which enable single Ag NPs to serve as nanoscale imaging probes to study size-dependent efflux kinetics of membrane transporters in real time and offer the unique opportunity to better understand molecular mechanisms of multidrug resistance.

Results and discussion

Synthesis and characterization of stable and purified Ag NPs (97 ± 13 nm)

We have synthesized the Ag NPs as described previously and in Method.[20,24,33] We purified the NPs by washing them with nanopure deionized (DI) water using centrifugation to remove any residual chemicals from the synthesis. The purified Ag NPs were stable in DI water for months, as we reported previously.[20,24,33] The high-resolution transmission electron microscopy (HRTEM) images and histogram of size distribution of single NPs show the polygon NPs with average sizes of (97 ± 13) nm, ranging from 72 to 147 nm with aspect ratios of 0.97–3.9 (Fig. 1A and B). The sizes of the NPs were determined by averaging the length and width of individual NPs. The dark-field optical images of single Ag NPs and their representative LSPR spectra (Fig. 1C and D) show individual plasmonic green, green-yellow, yellow, and red NPs, with peak wavelengths (full-width-at-half-maximum), λ_{max} (FWHM), of 521 (145), 536 (118), 560 (106), and 657 (114) nm, respectively.

The cells (*B. subtilis*) need to be incubated with culture media or PBS buffer in order to maintain their viability. Typically, accumulation and efflux kinetics of multidrug membrane transporters (efflux pumps) in bacterial cells (Gram-negative or Gram positive bacteria) have been carried out in the buffer solution (PBS buffer), but not in the cell culture medium.[10,34–38] This approach allows the given concentrations and stages of the cells (*e.g.*, $OD_{600\ nm} = 0.1$) to be incubated with given concentrations of fluorescence molecules (substrates), and enable the study of the dependence of accumulation and efflux kinetics of membrane transporters on substrate concentrations and on the expression level of membrane transporters.[10,34–38]

To probe the pore sizes of membrane transporters and to study size-dependent efflux kinetics of single membrane transporters of single live cells in PBS buffer using the size-dependent LSPR spectra of single NPs, we first characterized the stability (non-aggregated) of Ag NPs in the buffer (0.5 mM phosphate buffered saline, 1.5 mM NaCl) over time using UV-vis absorption spectroscopy and dynamic light scattering (DLS), to ensure that the LSPR spectra of single NPs remain unchanged during the entire duration of the experiment. The UV-vis absorption spectra of purified Ag NPs before and after their incubation with the buffer for 24 h remained unchanged with a peak absorbance of 1.9 at 505 nm and a shoulder peak of an absorbance of 1.6 at 419 nm (Fig. 2A). The size distributions of the NPs characterized using DLS show their average sizes at (89 ± 17) nm and (92 ± 19) nm (Fig. 2B) before and after their incubation with the buffer for 24 h, respectively. The results show the larger sizes of the NPs after the 24 h incubation, which is likely attributed to the solvation of NPs with water. The diameters of NPs measured in solution using DLS are slightly smaller than those determined under vacuum using HRTEM,

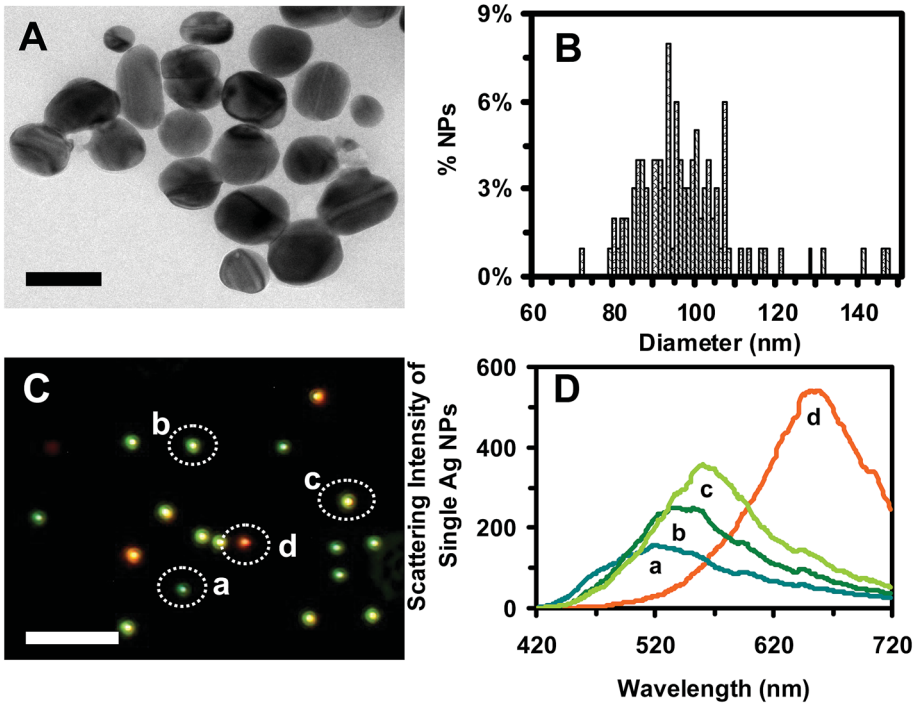

Fig. 1 Characterization of size and optical properties of single Ag NPs. (A) HRTEM images of single Ag NPs shows polygon shaped NPs. (B) Histograms of the size distribution of single Ag NPs measured by HRTEM shows an average diameter of 97 ± 13 nm, which was determined by averaging the length and width of each NP. (C) Representative dark-field optical image of single Ag NPs shows individual plasmonic green, green-yellow, yellow, and red NPs with (D) LSPR spectra at λ_{max} (FWHM): (a) 521 (145), (b) 536 (118), (c) 560 (106), and (d) 657 (114) nm, respectively. Scale bars are 100 nm in (A) and 2 μm in (C). The scale bar in (C) shows the distances among single NPs, but not their sizes, due to optical diffraction limit.

which is likely attributed to the different ways of calculation of sizes by TEM and DSL. Taken together, the results in Fig. 2 show that purified Ag NPs are stable in the buffer solution for 24 h. In this study, we present the sizes of NPs (97 ± 13 nm) using those measured by HRTEM.

Real-time imaging of efflux kinetics of single membrane transporters in single live cells

The representative dark-field optical images of the cells (WT, Ct-BmrA-EGFP and ΔBmrA) with single intracellular and extracellular NPs in Fig. 3 and S1† show cross-sections of single rod-like bacterial cells with 2 μm in length and 0.5 μm in width. The dark-field images show that the top and bottom membranes of single live cells are invisible under dark-field illumination and demonstrate that the focal plane (depth of field at 190 nm) of dark-field microscope enables us to image the thin-layer sections of single live cells with single NPs.

The sizes of the NPs and thickness of the cellular membrane (9 nm) are under optical diffraction limit (~200 nm). Therefore, the NPs appear to be on the membrane and stick outside the cells due to the higher scattering intensity of the NPs than the cell membrane. We use the scattering intensity of single NPs to determine intracellular and extracellular NPs. For intracellular NPs to be imaged by the detector, the dark-field microscope illumination needs to pass through the cellular membrane, and scattering of intracellular NPs needs to pass through the membrane to reach the detector. The cellular membrane absorbs photons and lowers scattering intensity of intracellular NPs. Thus, they look dimmer than the NPs outside the cells. The scattering intensity of the extracellular NPs on the membrane includes the scattering intensity of both NPs and cellular membrane. Thus, they look brighter and show higher scattering intensity. These distinctive features enable us to distinguish between the intracellular and extracellular NPs, which have been validated by imaging ultra-thin sections of cells using TEM.[25] The intracellular NPs are dimmer and blurry than NPs in solution (Fig. 3B-a and S1-b†). In contrast, the extracellular NPs are radiating and much brighter than NPs in solution (Fig. 3B-b and S1-c†).

Using the distinctive LSPR spectra (colors) of single Ag NPs, we effectively identified single Ag NPs over any other possible cellular debris and vesicles, which do not possess plasmonic properties and thereby appear white under dark-field illumination. The representative LSPR spectra of single Ag NPs in Fig. 3C show their peak wavelength (λ_{max}) at 540 (green), 552 (green) and 578 nm (yellow-green). We determined their sizes as 84, 91 and 100 nm in diameter, respectively, using their size-dependent LSPR spectra and the calibration curves of λ_{max} of LSPR spectra of single NPs *versus* their sizes, as we reported previously.[20,24]

Study of dependence of accumulation rates of NPs on expression level of BmrA

To determine whether BmrA are responsible for extrusion of NPs out of live cells, we used three BmrA cell strains (WT, Ct-BmrA-EGFP, ΔBmrA) to study the dependence of accumulation kinetics of intracellular NPs upon the expression level of

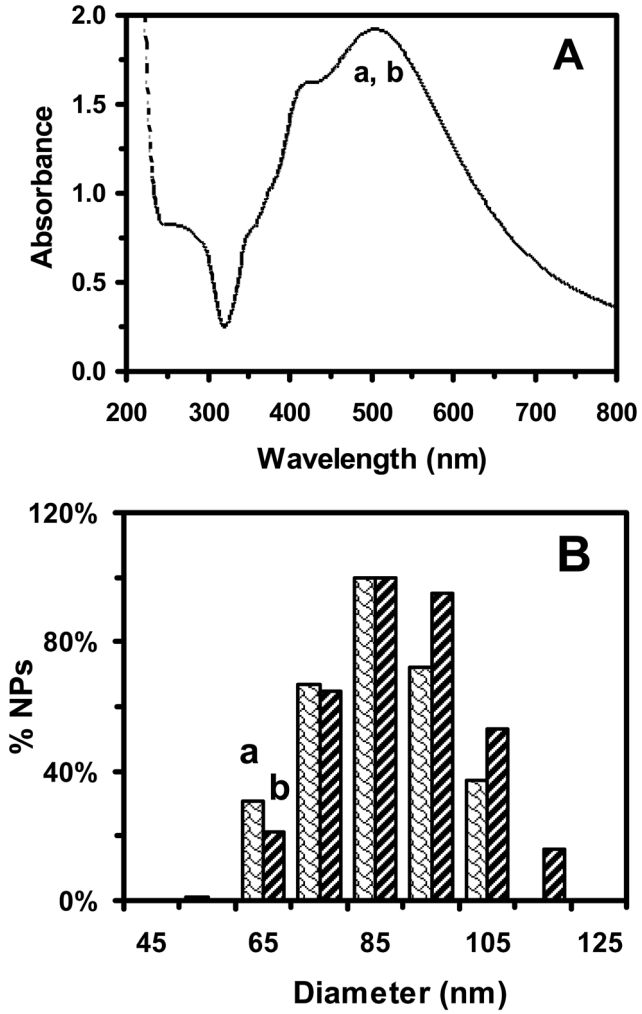

Fig. 2 Characterization of stability of Ag NPs (97 ± 13 nm) in the PBS buffer (0.5 mM phosphate buffer, 1.5 mM NaCl, pH = 7.0). (A) UV-visible absorption spectra (C_{NPs} = 3.7 pM) of the Ag NPs at (a) 0 h and (b) 24 h, show peak absorbance of 1.9 at 505 nm (FWHM = 150 nm) and a shoulder peak with a peak absorbance of 1.6 at 419 nm (FWHM = 93 nm). (B) Sizes of NPs in the PBS buffer measured using DLS show average diameters of (a) 89 ± 17 nm at 0 h and (b) 92 ± 19 nm at 24 h, indicating that the sizes of Ag NPs in the PBS buffer remain essentially unchanged and they are stable in PBS buffer for 24 h.

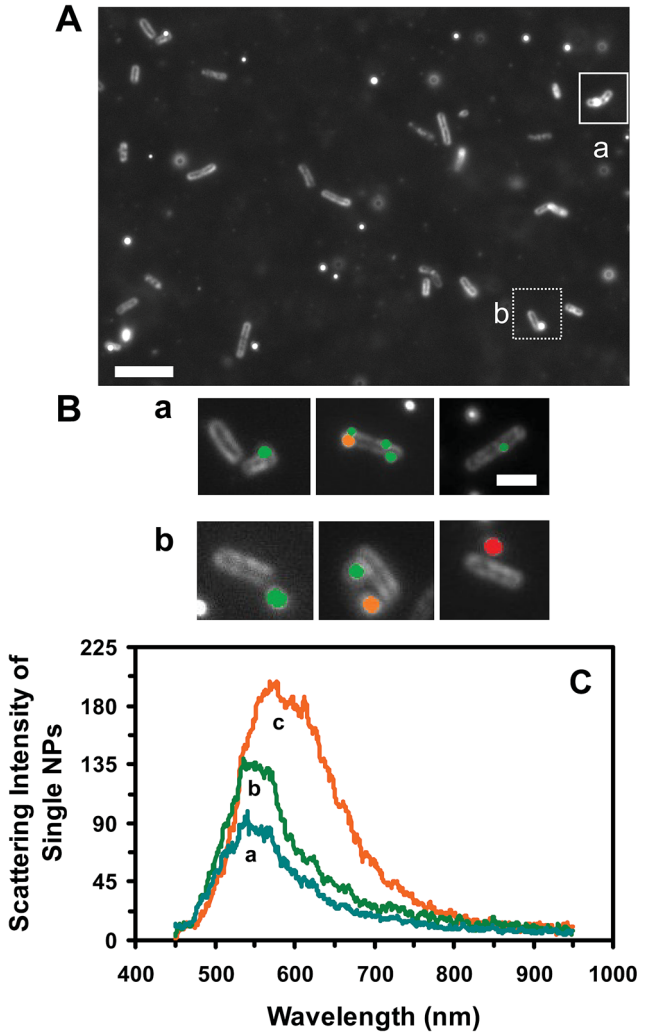

Fig. 3 Imaging of single intracellular and extracellular Ag NPs in single live cells using DFOMS. (A) Representative images of individual WT cells incubated with 3.7 pM Ag NPs show: (a) intracellular and extracellular NPs. (B) Zoom-in images of single cells show (a) intracellular and (b) extracellular NPs. (C) LSPR spectra of single NPs show peak wavelength (FWHM) at (a) 540 (96), (b) 552 (92) and (c) 578 (137) nm. The plasmonic colors of the NPs in (B) were characterized using their LSPR spectra in (C) and their pseudo colors were added into the images based upon their spectra. The scale bar is 6 μm in (A) and 2 μm in (B). Representative images of single cells (Ct-BmrA-EGFP and ΔBmrA) incubated with the NPs are shown in the ESI.†

BmrA in bulk live cells at single live cell resolution. The results in Fig. 4 show that ΔBmrA cells (strain of deleted BmrA) accumulate the highest amount of the intracellular NPs over time and exhibit the highest accumulation rate (slope of the plot) of intracellular NPs for each respective concentration of the NPs, while the Ct-BmrA-EGFP cells with the over-expression of Ct-BmrA-EGFP show the lowest accumulation amount and the lowest accumulation rate of intracellular NPs. Interestingly, the Ct-BmrA-EGFP cells with over-expression of Ct-BmrA-EGFP show only slightly lower accumulation amount and accumulation rate of intracellular NPs than WT, which could be attributed to the potential steric effects of EGFP.

We observed the similar dependence of accumulation rates of NPs on expression level of BmrA for all three concentrations of NPs (Table 1). For example, at the first 10.5 min incubation of the cells with 3.7 pM NPs, the accumulation rates of intracellular NPs in ΔBmrA, WT and Ct-BmrA-EGFP are 19.7, 6.8 and 5.4 intracellular NPs per min, respectively (Fig. 4A). At the first 10.5 min incubation of the cells with 1.85 pM NPs, the accumulation rates of intracellular NPs in ΔBmrA, WT and Ct-BmrA-EGFP are 12.2, 6.2 and 5.4 intracellular NPs per min, respectively (Fig. 4B). At the first 10.5 min incubation of the cells with 0.93 pM Ag NPs, the accumulation rates of intracellular NPs in ΔBmrA, WT and Ct-BmrA-EGFP are 6.9, 2.0 and 1.3 intracellular NPs per min, respectively (Fig. 4C).

The results suggest that WT and Ct-BmrA-EGFP cells extrude the intracellular NPs, leading to less accumulation of intracellular NPs than ΔBmrA cells. The results further demonstrate that

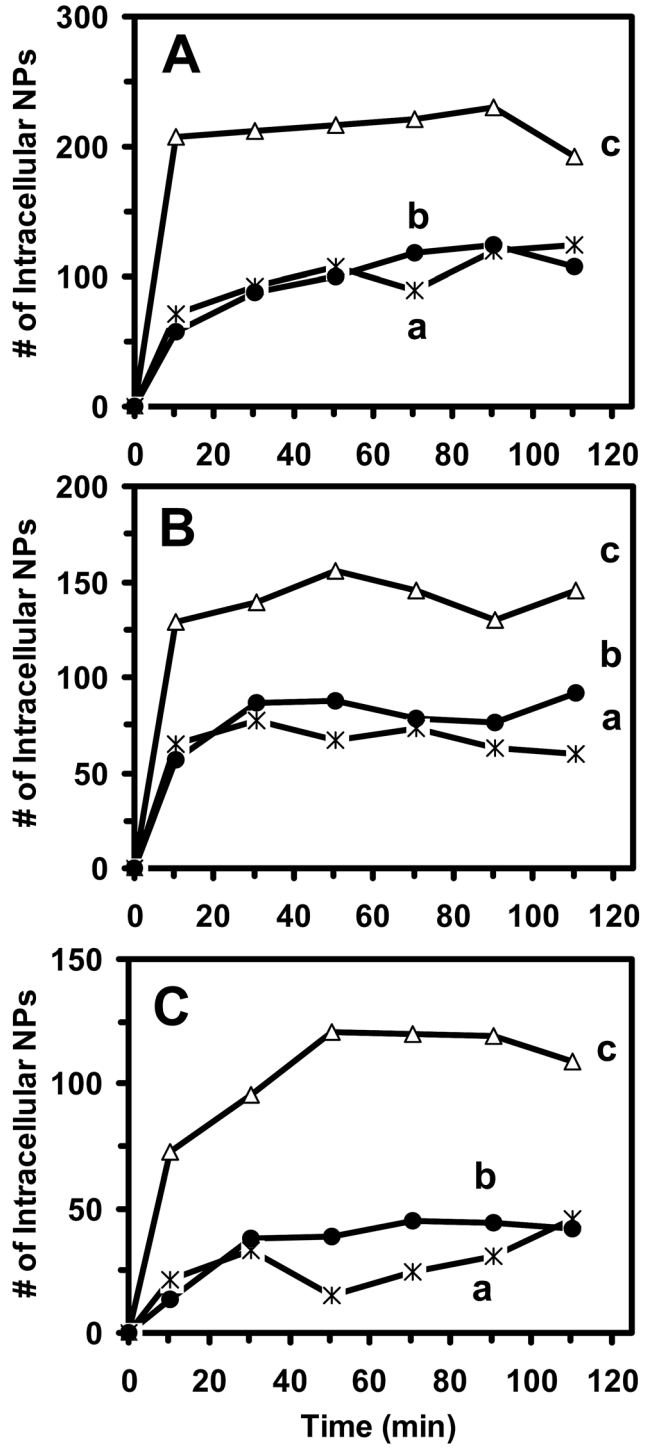

Fig. 4 Study of dependence of accumulation and efflux kinetics of single Ag NPs in single live cells on the expression level of BmrA. Plots of number of intracellular NPs in (a) WT (✱), (b) Ct-BmrA-EGFP (●) and (c) ΔBmrA (Δ) cells that were incubated with (A) 3.7, (B) 1.85, and (C) 0.93 pM NPs over 2 h. The points represent the sum of three repeated experiments and the lines are added to guide the trend. At each point (every 20 min), 300 cells are analyzed and presented at the central time point.

Ct-BmrA-EGFP maintain the efflux function of BmrA, similar to what we observed previously for the study of smaller Ag NPs (11.8 ± 2.6 nm) and fluorescence molecules (Hoechst 33 342).[14,29]

Table 1 Study of dependence of accumulation rates and number of intracellular single NPs in single live cells upon the expression level of BmrA and NP concentration

Diameter (nm)[a]	$C_{Ag\ NPs}$ (pM)	Accumulation rate (NPs min^{-1})[b]			Number of intracellular NPs[c]		
		WT	Ct[d]	ΔBmrA	WT	Ct[d]	ΔBmrA
97 ± 13	3.7	6.8	5.4	19.7	72	58	207
	1.85	6.2	5.4	12.2	65	57	128
	0.93	2.0	1.3	6.9	21	14	73

[a] Diameters of NPs measured by HRTEM. [b] Accumulation rates (slopes of the plots) at the first 10.5 min incubation in Fig. 4. [c] Number of intracellular NPs accumulated in 300 live cells during the first 10.5 min incubation. [d] Ct-BmrA-EGFP: cells with the over-expression of C-terminus BmrA fused with EGFP.[14,29]

The sizes of NPs (84–100 nm) are about a hundred times larger than conventional antibiotics. Such large substrates can be extruded by BmrA membrane transporter. Note that endocytosis, pinocytosis and exocytosis are not responsible for the transport of NPs in and out of the bacterial cells (*B. subtilis*) because they do not exist in prokaryotes (bacterial cells, *B. subtilis*). Unlike fluorescence probes, size-dependent plasmonic NPs offer size information about the membrane permeability and substrates of the membrane transporters and enable us to determine the size-dependent efflux kinetics of multidrug membrane transporters.

Study of concentration-dependent accumulation rates of single NPs in single live cells

We further characterized molecular mechanisms of entry of single NPs into single live cells, and determined whether the NPs share the same characteristics of pump substrates (antibiotics), such as concentration-dependent efflux kinetics. The results in Fig. 5 and Table 1 show that the number of intracellular NPs highly depends upon NP concentrations for all three strains (WT, Ct-BmrA-EGFP, ΔBmrA), and the number of intracellular NPs increases as the NP concentration increases. The number of intracellular NPs and their accumulation rates in ΔBmrA increase nearly proportionally with the NP concentration. As the concentration of NPs increases from 0.93, to 1.85 and 3.7 pM, the number of intracellular NPs accumulated in single live ΔBmrA cells increase from 73, to 128 and 207 during their 10.5 min incubation, showing the accumulation rates of 6.9, 12.2 and 19.7 NPs per min, respectively.

In contrast, the number of intracellular NPs and their accumulation rates in WT and Ct-BmrA-EGFP do not increase nearly proportionally with the NP concentration. For example, as the concentration of NPs increases from 0.93, to 1.85 and 3.7 pM, the number of intracellular NPs accumulated in single live WT cells increase from 21, to 65 and 72 during their 10.5 min incubation, showing the accumulation rates of 2.0, 6.2 and 6.8 NPs per min, respectively. As the concentration of NPs increases from 0.93, to 1.85 and 3.7 pM, the number of intracellular NPs accumulated in single live Ct-BmrA-EGFP cells increase from

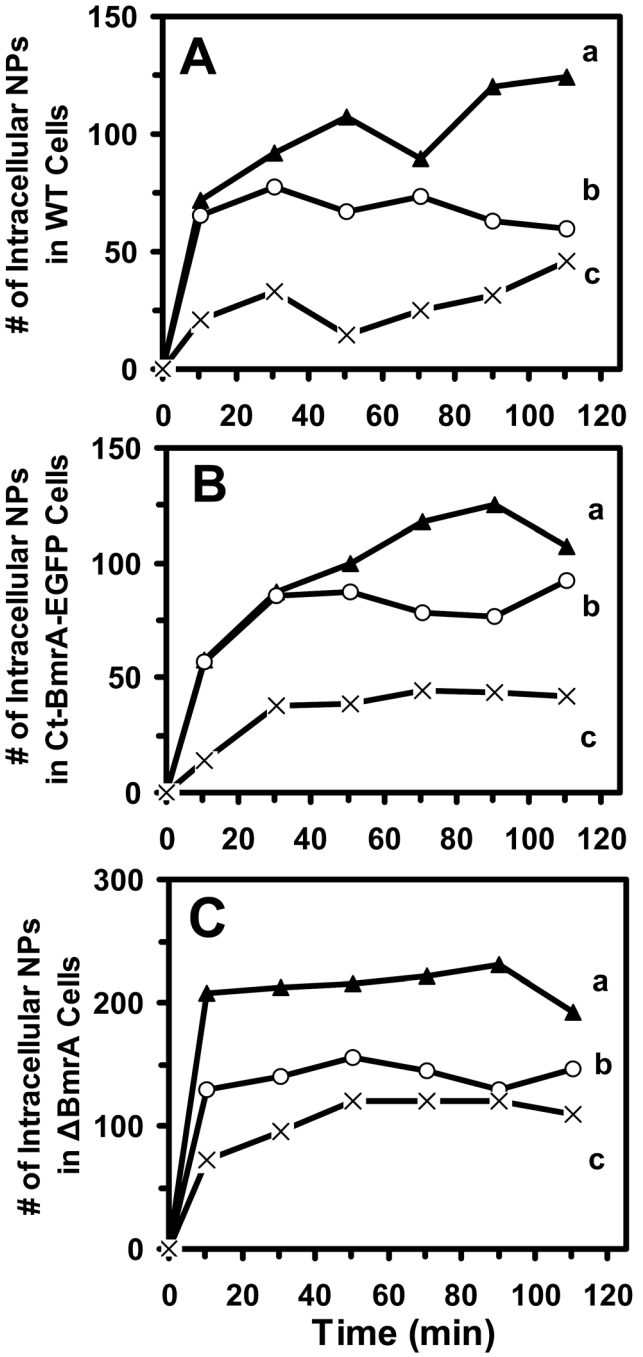

Fig. 5 Study of concentration-dependent accumulation and efflux kinetics of single Ag NPs in single live cells. Plots of number of intracellular NPs in (A) WT, (B) Ct-BmrA-EGFP and (C) ΔBmrA cells that were incubated with (a) 3.7, (b) 1.85, and (c) 0.93 pM NPs for 2 h. The points represent the sum of three repeated experiments and the lines are added to guide the trend. At each point (every 20 min), 300 cells are analyzed and presented at the central time point.

14, to 57 and 58 during their 10.5 min incubation, showing the accumulation rates of 1.3, 5.4 and 5.4 NPs per min, respectively.

These interesting results suggest that the efflux rates highly depend upon the concentration of the intracellular NPs in WT and Ct-BmrA-EGFP cells and they could increase much more rapidly than the diffusion rates at the higher concentration and lead to the lower concentration of intracellular NPs. In other words, the passive diffusion rates of the NPs into the cells increase proportionally with the NP concentration, while the efflux rates do not and they increase much more rapidly at the higher concentration. Consequently, we observed an equilibrium (saturated) accumulation rates of the NPs in WT and Ct-BmrA-EGFP cells that are nearly independent to the NP concentration, as the NP concentration increases from 1.85 to 3.7 pM, as shown in Fig. 5 and Table 1.

Taken together, the results suggest that passive diffusion is very likely responsible for the transport of extracellular NPs into the cells, similar to passive diffusion of antibiotics into the cells, and BmrA extrudes the NPs out of the cells, leading to the lower accumulation of intracellular NPs in WT and Ct-BmrA-EGFP cells. Interestingly, the results further suggest that the efflux rates of BmrA could be triggered and increased substantially by higher diffusion rates of NPs into the cells upon incubation with higher NP concentration, which maintains low intracellular NPs and achieve its biological function to protect live cells. Such smart efflux pump (BmrA) could be highly responsive to its substrate concentration and be tunable. To our knowledge, such smart functions have not been reported previously.

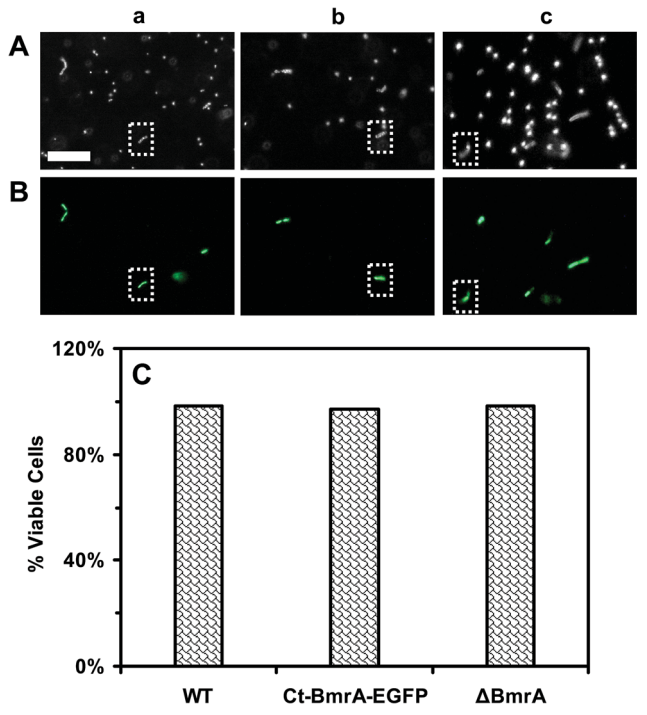

Fig. 6 Characterization of the viability of single cells using live/dead *Bac*Light viability and counting assay. (A) Dark field optical image and (B) fluorescence image of single (a) WT, (b) Ct-BmrA-EGFP, and (c) ΔBmrA cells that had been incubated with 3.7 pM NPs for 2 h show that the cells with or without intracellular NPs emit the green fluorescence of SYTO9 (λ_{max} = 520 nm), but not red fluorescence, indicating that they are viable. (C) Plots of percentage of viable cells incubated with NPs for 2 h show that 97–98% of the cells (WT, Ct-BmrA-EGF or ΔBmrA) are alive. The scale bar is 8 μm.

Characterization of viability of single cells

We characterized the viability of single cells with the NPs to ensure that the accumulation of intracellular NPs is not attributed to the disintegration of cell membrane of the dead cell. The cells (WT, BmrA-EGFP, ΔBmrA) incubated with NPs throughout the duration of the experiments were characterized using live/dead *Bac*Light viability and counting assay. The assay uses SYTO9 nucleic acid stain and propidium iodide to detect live and dead cells, respectively.[39] Note that SYTO9 enter into live bacterial cells and lead to the green fluorescence ($\lambda_{max} = 520$ nm), which enables assay of viable cells. In contrast, propidium iodide can only enter into the dead bacterial cells due to the disintegration of the cellular membrane of the dead cells, and lead to red fluorescence ($\lambda_{max} = 610$ nm), which enables assay of the dead cells. Representative optical images of the cells (WT, Ct-BmrA-EGFP, ΔBmrA) incubated with 3.7 pM Ag NPs for 2 h show the cells with and without NPs (Fig. 6A). Their fluorescence images display the green fluorescence, indicating that the cells with and without NPs are alive (Fig. 6B).

We determined the number of live and dead cells and presented the percentage of the viable cells by dividing the number of live cells with the total number of the cells. The result shows that 97–98% of the cells of each strain are alive (Fig. 6C), which indicates that the selected Ag NP concentration (3.7 pM) are biocompatible to the cells, and the NPs are well suited to serve as optical imaging probes for real-time study of membrane transporters of single live cells.

Summary

In summary, we have prepared the purified Ag NPs (97 ± 13 nm), which are stable (non-aggregation) in the PBS buffer over 24 h. We found that the NPs with concentrations up to 3.7 pM are biocompatible with the cells and can be used as photostable optical imaging probes to study efflux kinetics of BmrA (ABC) membrane transporters in single live cells. This study shows the high dependence of accumulation of the intracellular single Ag NPs in single live cells (WT, Ct-BmrA-EGFP, ΔBmrA) upon the expression level of BmrA. The results indicate the highest accumulation rates and number of intracellular NPs in ΔBmrA cells (deletion of BmrA), and the lowest ones in Ct-BmrA-EGFP cells (over-expression of Ct-BmrA-EGFP), suggesting that BmrA and Ct-BmrA-EGFP extrudes the NPs out of the cells. Furthermore, the accumulation rates and the number of intracellular NPs in ΔBmrA cells increase nearly proportionally with the NP concentration, while those in WT and Ct-BmrA-EGFP cells do not, suggesting that the NPs enter the cells *via* passive diffusion and be extruded out of cells by BmrA (efflux pump), similar to the well-known conventional pump substrates (antibiotics). Interestingly, the results suggest that the efflux rates highly depend upon the concentration of the intracellular NPs in WT and Ct-BmrA-EGFP cells and could increase much more rapidly than the diffusion rates at the higher concentration. Consequently, it leads to equilibrium (saturated) accumulation rates of the NPs in WT and Ct-BmrA-EGFP cells that are nearly independent to the NP concentration, as the NP concentration increases from 1.85 to 3.7 pM. To our knowledge, such smart functions have not been reported previously. Taken together, these results suggest that the NPs share the same transport mechanisms of pump substrates (antibiotics) and hence can serve as effective optical imaging probes to study the size-dependent efflux kinetics of membrane transporters in single live cells in real time. Unlike fluorescence imaging probes, single Ag NPs possess photostability and size-dependent LSPR spectra and they can be used to mimic various sizes of antibiotics (drugs) to quantitatively study the size-dependent efflux kinetics of membrane transporters of single live cells at nm resolution in real-time for better understanding of multi-drug resistance. Further study is underway to depict efflux pathway of such large substrates (84–100 nm NPs) by BmrA membrane transporter.

Materials and methods

Reagents and supplies

Sodium citrate (99%), $AgClO_4$ (99%) and $NaBH_4$ (98%) were purchased from Sigma Aldrich, and live/dead *Bac*Light viability and counting assay was purchased from Invitrogen. All reagents were used as received. The nanopure DI water (18 MΩ water, Barnstead) was used to prepare all solutions and rinse glassware.

Synthesis and characterization of stable and purified Ag NPs (97 ± 13 nm)

The Ag NPs (97 ± 13 nm) were synthesized and purified as we described previously.[20,24,33] Briefly, we rapidly added sodium citrate (20 mL, 34 mM in nanopure DI water) into $AgNO_3$ (500 mL, 1.06 mM in DI water) under stirring and refluxing and continuously refluxed and stirred the mixture for 95 min, as the solution colors turned from colorless to different shades of yellow. We then stopped heating and continued refluxing and stirring the solution until it was cooled to room temperature. We then filtered the NP solution using 0.22 μm filters and washed the NPs three times with DI water using centrifugation (Beckman, JA-20) to remove any possible residual chemicals from NP synthesis to prepare purified Ag NPs. We dispersed the washed Ag NPs in the PBS buffer (0.5 mM phosphate buffer, 1.5 mM NaCl, pH = 7.0) and characterized the NP concentrations, the LSPR images and spectra of single NPs, and sizes of single NPs using UV-vis spectroscopy (Hitachi U-2010), dark-field optical microscopy and spectroscopy (DFOMS), HRTEM (JEOL, JEM-2100F), and DLS (Nicomp 380ZLS particle sizing system), respectively.

Our DFOMS is equipped with a dark-field optical microscope, which includes a dark-field condenser (oil 1.43–1.20, Nikon) and a 100× objective (Nikon Plan fluor 100× oil, iris, SL. N.A. 0.5–1.3, W.D. 0.20 mm) with a depth of field (focus) of 190 nm, a CCD camera (Micromax, Roper Scientific) and Multi-spectral Imaging System (Nuance, CRI).[40–42] The design and construction of DFOMS have been fully described in our previous studies.[22–29,40,41,43]

Cell lines and cell culture

The *Bacillus subtilis* cell lines using in this study are as follows: WT (BmrA) were purchased from Bacillus Genome Stock Center (BGSC), and ΔBmrA (previously named as Δ*yvcC* and ΔBmrA, mutant strain that is void of the BmrA) were provided by J. M. Jault.[37] The cell line of Ct-BmrA-EGFP (54A, a mutant with over expression level of BmrA with its C-terminal fused with EGFP) was constructed and characterized as we described previously.[14,29]

The cells were pre-cultured in an Erlenmeyer flask (250 mL) containing 20 mL of L-broth (LB) medium (1% tryptone peptone, 0.5% yeast extract, and 0.5% NaCl, pH = 7.2) in a shaker (Lab-line Orbit Envivon-Shaker) (150 rpm, 37 °C) for 12 h. The cells (WT and ΔBmrA) in the LB medium were cultured for another 8 h, while Ct-BmrA-EGFP cells were cultured in the medium containing 1% xylose for another 8 h to ensure the full expression of EGFP. The cultured cells were harvested using centrifugation (Beckman Model J2-21 Centrifuge, JA-14 rotor, at 7500 rpm, 23 °C, 10 min), washed with the PBS buffer three times, and finally re-suspended in the PBS buffer. We adjusted the final concentration of the cells to $OD_{600\ nm} = 0.1$, and used it for the entire study.

Imaging of single NPs in single live cells and cell viability

The cell suspension ($OD_{600\ nm} = 0.1$) was incubated with 0.93, 1.85 or 3.7 pM NPs in the PBS buffer for 2 h. We sampled the mixture into a freshly prepared microchamber every 20 min and imaged the cells with the NPs over time. This approach permitted us to image massive amount of cells (2100 cells) for each sample to gain sufficient statistics for probing the accumulation and efflux kinetics of NPs in bulk cells at single cell resolution. We determined the number of intracellular NPs and plotted them *versus* time to measure accumulation rates of single NPs in the cells over time (accumulation rate = slope of the plot).

After the 2 h incubation, we characterized the viability of the cells using live/dead *Bac*Light bacterial viability and counting assay.[39] We imaged the cells using dark-field optical microscopy and epi-fluorescence microscopy, and counted the green fluorescence cells (peak wavelength of fluorescence spectra of SYTO9, $\lambda_{max} = 520$ nm) and red fluorescence cells (peak wavelength of fluorescence spectra of propidium iodide, $\lambda_{max} = 610$ nm) as live and dead cells, respectively.

It is worth noting that, in order to determine the accumulation rates of single NPs in the cells over time, the number of the cells and NP concentration must remain unchanged over time. Thus, the PBS buffer (but not cell culture medium) was used to suspend the bacterial cells for the study of accumulation kinetics of pump substrates over time, as those reported previously.[14,15,24,25,33,35,37] Note that the cells would grow in the culture medium, and the number of the cells would change over time, making the study of the accumulation rates of single NPs in the cells over time impossible. Our studies demonstrate that the bacterial cells remain alive and retain their efflux functions in the PBS buffer, as shown in Fig. 4–6 and as reported previously.[14,15,24,25,33,35,37]

Data analysis and statistics

We acquired ten representative images of each cell suspension incubated with 0.93, 1.85 or 3.7 pM Ag NPs every 20 min for 2 h to study accumulation rates of intracellular NPs in single live cells. Therefore, a minimal of ~100 cells was imaged every 20 min, and 700 cells were studied over 2 h for each measurement. Each experiment was repeated three times. Thus, 2100 cells were studied for each sample with 300 cells at each 20 min which allowed us to gain sufficient statistics for probing accumulation rates and efflux kinetics of bulk cells at single cell resolution. Unlike bulk measurement, this study was carried out at single cell resolution. Thus, the data in Fig. 4 and 5 and Table 1 represent the sum of three repeated experiments for 300 cells at each 20 min, instead of average of 100 cells with standard deviations.

Acknowledgements

This work is supported in part by NSF (CBET 0507036 and CBET 1450936) and NIH (R01 GM0764401). Browning, Lee and Nallathamby are grateful for the support of NIH-GRAS (R01 GM076440S1), NSF-GRAS (CBET 0940923), and Dominion Scholar Fellowship, respectively. All work was done in the Xu lab at ODU. LMB, KJL and PKC conducted the study of transport of single NPs and data analysis; PDN synthesized and characterized the NPs; SW participated in data analysis; JMJ provided ΔBmrA bacterial cell line and helpful discussion. XHNXu (principal investigator) directed the research project, oversaw the experiments, reviewed and interpreted data, and wrote the manuscript.

References

1 S. P. Cole, *J. Biol. Chem.*, 2014, **289**, 30880–30888.
2 S. K. Nigam, *Nat. Rev. Drug Discovery*, 2015, **14**, 29–44.
3 M. M. Gottesman, S. V. Ambudkar and D. Xia, *Nat. Biotechnol.*, 2009, **27**, 546–547.
4 C. F. Higgins, *Res. Microbiol.*, 2001, **152**, 205–210.
5 L. W. Hung, I. X. Wang, K. Nikaido, P. Q. Liu, G. F. Ames and S. H. Kim, *Nature*, 1998, **396**, 703–707.
6 K. P. Locher, A. T. Lee and D. C. Rees, *Science*, 2002, **296**, 1091–1098.
7 A. L. Davidson and J. Chen, *Annu. Rev. Biochem.*, 2004, **73**, 241–268.
8 I. B. Holland and M. A. Blight, *J. Mol. Biol.*, 1999, **293**, 381–399.
9 H. Morjani, N. Aouali, R. Belhoussine, R. J. Veldman, T. Levade and M. Manfait, *Int. J. Cancer*, 2001, **94**, 157–165.
10 P. G. Mortimer and L. J. Piddock, *J. Antimicrob. Chemother.*, 1991, **28**, 639–653.
11 C. Orelle, F. Gubellini, A. Durand, S. Marco, D. Levy, P. Gros, A. Di Pietro and J. M. Jault, *Biochemistry*, 2008, **47**, 2404–2412.
12 C. Steel, Q. Wan and X. H. Xu, *Biochemistry*, 2004, **43**, 175–182.

13 X.-H. N. Xu, W. J. Brownlow, S. Huang and J. Chen, *Biochem. Biophys. Res. Commun.*, 2003, **305**, 79–86.
14 F. Ding, K. Lee, A. Vahedi-Faridi, T. Huang and X.-H. N. Xu, *Anal. Bioanal. Chem.*, 2011, **400**, 223–235.
15 F. Ding, K. J. Lee, A. Vahedi-Faridi, H. Yoneyama, C. J. Osgood and X. H. N. Xu, *Analyst*, 2014, **139**, 3088–3096.
16 I. I. Serysheva, S. J. Ludtke, M. L. Baker, Y. Cong, M. Topf, D. Eramian, A. Sali, S. L. Hamilton and W. Chiu, *Proc. Natl. Acad. Sci. U. S. A.*, 2008, **105**, 9610–9615.
17 P. F. Fribourg, M. Chami, C. O. Sorzano, F. Gubellini, R. Marabini, S. Marco, J. M. Jault and D. Lévy, *J. Mol. Biol.*, 2014, **426**, 2059–2069.
18 T. Huang and X.-H. N. Xu, *J. Mater. Chem.*, 2010, **20**, 9867–9876.
19 U. Kreibig and M. Vollmer, in *Optical Properties of Metal Clusters*, Springer, Berlin, 1995, pp. 14–123.
20 P. D. Nallathamby, T. Huang and X.-H. N. Xu, *Nanoscale*, 2010, **2**, 1715–1722.
21 K. L. Kelly, E. Coronado, L. L. Zhao and G. C. Schatz, *J. Phys. Chem. B*, 2003, **107**, 668–677.
22 L. M. Browning, K. J. Lee, T. Huang, P. D. Nallathamby, J. Lowman and X.-H. N. Xu, *Nanoscale*, 2009, **1**, 138–152.
23 K. J. Lee, P. D. Nallathamby, L. M. Browning, C. J. Osgood and X.-H. N. Xu, *ACS Nano*, 2007, **1**, 133–143.
24 P. D. Nallathamby, K. J. Lee, T. Desai and X.-H. N. Xu, *Biochemistry*, 2010, **49**, 5942–5953.
25 X.-H. N. Xu, W. J. Brownlow, S. V. Kyriacou, Q. Wan and J. J. Viola, *Biochemistry*, 2004, **43**, 10400–10413.
26 X.-H. N. Xu, J. Chen, R. B. Jeffers and S. V. Kyriacou, *Nano Lett.*, 2002, **2**, 175–182.
27 P. D. Nallathamby, K. J. Lee and X.-H. N. Xu, *ACS Nano*, 2008, **2**, 1371–1380.
28 S. V. Kyriacou, W. J. Brownlow and X. H. N. Xu, *Biochemistry*, 2004, **43**, 140–147.
29 K. J. Lee, L. M. Browning, T. Huang, F. Ding, P. D. Nallathamby and X.-H. N. Xu, *Anal. Bioanal. Chem.*, 2010, **397**, 3317–3328.
30 C. Aguilar, H. Vlamakis, R. Losick and R. Kolter, *Curr. Opin. Microbiol.*, 2007, **10**, 638–643.
31 Y. Quentin, G. Fichant and F. Denizot, *J. Mol. Biol.*, 1999, **287**, 467–484.
32 U. Völker and M. Hecker, *Cell. Microbiol.*, 2005, **7**, 1077–1085.
33 K. J. Lee, P. D. Nallathamby, L. M. Browning, T. Desai, P. Cherukui and X.-H. N. Xu, *Analyst*, 2012, **137**, 2973–2986.
34 S. V. Kyriacou, M. E. Nowak, W. J. Brownlow and X.-H. N. Xu, *J. Biomed. Opt.*, 2002, **7**, 576–586.
35 A. Ocaktan, H. Yoneyama and T. Nakae, *J. Biol. Chem.*, 1997, **272**, 21964–21969.
36 E. Steinfels, C. Orelle, O. Dalmas, F. Penin, B. Miroux, A. Di Pietro and J. M. Jault, *Biochim. Biophys. Acta*, 2002, **1565**, 1–5.
37 E. Steinfels, C. Orelle, J. R. Fantino, O. Dalmas, J. L. Rigaud, F. Denizot, A. Di Pietro and J. M. Jault, *Biochemistry*, 2004, **43**, 7491–7502.
38 X.-H. N. Xu, Q. Wan, S. V. Kyriacou, W. J. Brownlow and M. E. Nowak, *Biochem. Biophys. Res. Commun.*, 2003, **305**, 941–949.
39 M. Berney, F. Hammes, F. Bosshard, H. U. Weilenmann and T. Egli, *Appl. Environ. Microbiol.*, 2007, **73**, 3283–3290.
40 T. Huang, P. D. Nallathamby and X.-H. N. Xu, *J. Am. Chem. Soc.*, 2008, **130**, 17095–17105.
41 P. D. Nallathamby and X.-H. N. Xu, *Nanoscale*, 2010, **2**, 942–952.
42 T. Huang and X.-H. N. Xu, *Nanoscale*, 2011, **3**, 3567–3572.
43 T. Huang, P. D. Nallathamby, D. Gillet and X.-H. N. Xu, *Anal. Chem.*, 2007, **79**, 7708–7718.